Implementation and validation of a bulk microphysical model of moisture transport in a pressure based CFD solver

Norbert Rácz[*] and **Gergely Kristóf**

Department of Fluid Mechanics,
Budapest University of Technology and Economics (BME),
Bertalan L. u. 4-6, H-1111 Budapest, Hungary
E-mails: racz@ara.bme.hu; kristof@ara.bme.hu

[*]*Corresponding author*

Abstract—We study wet cooling tower plume formation involving mesoscale meteorological effects (such as stratification or compressibility). This was achieved by incorporating transformations and volume source terms into a pressure based computational fluid dynamics (CFD) solver (ANSYS-FLUENT). Moisture dynamics is taken into account with a bulk microphysical model that was recently implemented into the solver.

This model has been validated against known numerical solutions of idealized two-dimensional dry and wet thermals. In particular, the overall thermal profile and the liquid water concentration field indicated good model performance. Model performance has also been compared with measurements for the formation of a large wet cooling tower plume. Simulations are encouraging with regard to the predictability of cumulus like plume structures with complex thermal stratification, the overall liquid water content along the plume axis, and also the turbulent fluctuations caused by the vertical movements in the plume.

The advantage of this approach is that a uniform physical description can be used for close- and far-field flow by using a single unstructured mesh with local refinements. This allows for investigating the finely structured microscale flow phenomena around complex orographic features in a single framework.

Key-words: humidity transport, wet adiabatic processes, phase change, rising thermal, wet cooling tower plume

1. Introduction

A clear trend can be seen in the development of mesoscale meteorological codes towards the usage of higher resolution numerical models incorporating multiple physical effects in order to better describe the atmosphere, give higher resolution models for urban environments, or give higher fidelity forecasting. This is well reflected in the "urbanization" of mesoscale meteorological models (*Yamada*, 2003; *Otte et al.*, 2004; *Ooka et al.*, 2010), where microscale physical effects are introduced.

Another approach for multi-scale modeling is when computational fluid dynamical (CFD) solvers are adapted to handle mesoscale effects. The purpose of this paper is to enhance the latter approach.

General purpose CFD solvers are already widely used in modeling the ventilation of urban areas (*Mochida et al.*, 1997; *Balczó et al.*, 2011; *Kristóf* and *Balogh*, 2010). These solvers are capable of handling complex topography, buildings and have a wide variety of turbulence and physical models, effective numerical techniques, and parallelization.

In order to handle mesoscale effects in a general purpose CFD solver, we have recently developed a method (*Kristóf et al.*, 2009). The atmospheric stratification, the Coriolis force, and baroclinicity are taken into account by using simple (scale and shift) transformations of state variables (pressure, density, temperature), vertical velocity, and altitude, and including additional source terms in the conservation equations. The model was successfully validated (*Kristóf et al.*, 2009). Further simulations by *Rácz et al.* (2013) were performed around more complex geometrical features, idealized barriers, and real terrain, demonstrating the capabilities of this CFD based approach.

The contribution of this paper is to extend our original 2009 model with a proper moisture (humidity transport and phase change) model. We validate this extended model with numerical solutions of idealized two-dimensional dry and wet thermals and experimental data for a full-scale three-dimensional wet cooling tower plume formation with different environmental stratifications.

Several researchers investigated the behavior of cooling tower plumes from different aspects in the past decades. Wet cooling towers are widely used in the power generation industry, since it is relative easy to build and cheap to operate especially in regions where limited water resources are available for cooling purposes (*Al-Waked* and *Behnia*, 2006).

Most of the earlier studies are from the early 1970s related to the design, construction, and operation of nuclear and coal fired power plants. The performance of cooling towers is an important topic as the energy demand is growing. Few percent increase in overall efficiency in power generation could lead to high amount of total energy savings. Therefore, number of researches investigated the effect of changes in environmental conditions to the tower performance. *Al-Waked* and *Behnia* (2006) and *Lohasz* and *Csaba* (2012)

studied the effects of crosswind, *Kloppers* and *Kröger* (2005), *Overcamp* and *Hoult* (1971), *Barber et al.* (1974) studied temperature and humidity inversion and other parameters with CFD methods under different operating conditions. These effects are important since they could lower the efficiency of cooling towers (*Wei et al.*, 1995).

The visibility was not a great concern at that time, instead the plume rise of dry and wet plumes were investigated (*Hanna*, 1972; *Weil*, 1974). Wet cooling towers, however, do not have much control over the visible plume. (*Tyagi et al.*, 2012) The exhaust of the tower is generally saturated, and during certain weather conditions, it cannot be absorbed completely by the surrounding air. As a result, it will appear as fog and visible to human eye.

Another important aspect regarding wet cooling tower operation is the prevention of the growth of legionella bacteria in the cooling water. The various legionella species are the cause of Legionnaires' disease in humans, and the transmission is via the exposure to aerosols. The bacteria could live and travel hundreds of meters or even kilometers from the source (*Greig et al.*, 2004) .

Nowadays, environmental impacts are becoming more and more important concentrating not only on toxic materials but also on the visibility of water vapor plumes. The reduction of visibility conditions, the local reduction of solar radiation, and the interaction with low level clouds, in particular the fog, are in concern nowadays. The latest literature review about cooling towers shows different options for reducing and manipulating the visible plume using hybrid cooling towers, wet–dry cooling towers, dry cooling towers, and so on, depending on the need and demand. The formation of a visible water vapor plume is directly related to the water mass fraction, temperature, exhaust velocity of the tower, and also ambient meteorological conditions. In more recent studies, *Wang et al.* (2007), *Xu et al.* (2008) and *Wang et al.* (2009) investigated the control and abatement of plumes emitted by large commercial buildings by reheating the exhaust with heat pumps or solar collectors. *Sturman* and *Zawar-Reza* (2011) predicted the yearly visibility of a stack plume of a planned industrial site with an atmospheric mesoscale pollution model (TAPM) by providing boundary conditions from the meteorological code. *Presotto et al.* (2005) investigated the possibility of reducing the plume visibility by lowering the exit temperature of a petrochemical refinery.

There is usually no contaminant involved, but there is a risk of the plume's material returning to the ground level causing local fogging, ice formation, or entrainment of saturated air into other adjacent towers. *Mokhtarzadeh-Dehghan et al.* (2006) and *Spillane* and *Elsum* (1983) investigated the occurrence of rain and fog and the possibility of plum blow-out by strong winds. Their investigation showed that the fog can extend to the ground in cases, where the plume interacts with the wake of the tower and the ambient temperature is very low.

Number of researchers worked on the effect of drift deposition as it could be objectionable due to human health hazards. Their purpose was to investigate

the effects of ambient conditions and absolute humidity, droplet output temperature, and the affected area (*Lucas et al.*, 2010). Drift of small water droplets from mechanical and natural draft cooling towers can contain salt particles, water treatment chemicals, and bacteria. *Meroney* (2006) recommends a CFD protocol to correct drift and deposition predictions provided by current analytic models to take into account building effects.

Wet cooling tower plumes can also play a role in the formation of different kinds of hydrometeors. *Campistron* (1987) and *Huff* (1972) studied snowfalls caused by cooling towers and they found that the rate of precipitation can even be enhanced by a factor of two.

The increasing computational power makes the CFD based approach more and more affordable. Several investigations showed that CFD models are valid in predicting the flow field, performance, or drift deposition predictions of micro scale flow around cooling towers (*Balczó et al.*, 2011; *Kristóf and Balogh*, 2010; *Meroney*, 2006). We have successfully extended the capabilities of CFD solvers (*Kristóf et al.*, 2009; *Rácz et al.*, 2013) in order to simulate atmospheric scale flows. In this paper, a further enhanced model version will be shown that is capable of predicting moist dynamics through the implementation of condensation and phase change models.

In the next chapter, an overview will be given about the existing tools for modeling plume dispersion and about their advantages and limitations, a short description of the mesoscale model extension that we have recently validated, and more details on the further developed model version that also takes into account moist dynamics. In the third and fourth chapters, the model validation will be shown against calculations with meteorological codes and field measurements followed by the conclusions.

2. Mathematical model

Theories for describing the heat, mass, and momentum transfer inside natural draft cooling towers have long been established by authors in the early 1900s. These works (*Lewis*, 1922; *Robinson*, 1923) include also heat transfer due to vaporization, and therefore, they are applicable to the prediction of wet tower performance. These analysis and simplifications are still in use today, and several numerical models have been developed based on this study in order to describe transfer processes inside cooling towers (*Al-Waked and Behnia*, 2006).

Wide range of model complexity can be found in the literature regarding the modeling of plume formation outside of the tower. These models include simpler algebraic models towards more complex integral models, atmospheric dispersion models, or CFD based approaches. Commonly used plume models are based on conservation equations describing the entrainment processes of ambient air along the plume axis.

Several authors (*Hanna*, 1976; *Hanna et al.*, 1982) studied the dynamics of plume motion and developed numerical models. *Slawson and Csanady* (1967), *Wigley and Slawson* (1971), and *Csanady* (1973) identified three phases, the initial, intermediate, and final phases of plume rise. They developed a rise model for jets that is also applicable to ambient conditions with stable stratification.

Widely used models, e.g., the analytical models of *Briggs* (1975, 1984) and *Weil* (1974) describe reasonably well the first phase of plume rise near the source, however, they are valid only for constant density gradient and wind speed (*Briggs*, 1984). With the detrainment concept of *Netterville* (1990), the transitional region and the leveling can also be described. *Davidson* (1989, 1994) developed a formulation that is able to predict both plume rise and dilution.

The entrainment is often modeled by using different empirical coefficients (*Schatzmann and Policastro*, 1984). One reason of difference between model results of different formulations is due to the differences in empirical coefficients applied to obtain the analytic solution.

Early models did not account for phase change of water during the plume development and neglect the effect of turbulence to the entrainment. *Gangoiti et al.* (1997) and *Janicke and Janicke* (2001) have developed Gaussian dispersion type models that included prediction of condensation and are also applicable to complex wind fields. Condensation and evaporation of droplets is important, since it changes buoyancy by introducing and removing latent heat during the rise and leveling. The lack of plume condensation causes the underestimation of plume rise in simpler models.

Another usual limitation is the improper handling of the complex atmospheric stratification and wind fields. Simplifications often assume winds depending only on the height above the ground, or constant wind speed and direction along the plume axis. In the case of complex input meteorological conditions data are often extrapolated from nearby meteorological stations to represent ambient conditions at the source. However, this causes accuracy problems (*Presotto et al.*, 2005). Simpler models could give good results in certain conditions when the lower few 100 meters of the atmosphere is linearly stratified. However, in the cases of high exhaust temperatures, the plume can penetrate deeply into the atmosphere crossing different layers with different lapse rates. This is typical for stack plumes of wet scrubbers with high exhaust temperatures.

The proper estimation of plume rise height is especially important when the deposition of plume particles or ground level concentration is to be calculated. *Policastro et al.* (1978) compared drift deposition models to experimental data and found that the existing models did not perform well.

The formulation of *Briggs* (1984) extended with empirical coefficients for plume trajectory are in use in environmental protection regulatory models (*Gangoiti et al.*, 1997). For short-range transport, the modifications to the EPA

Point, Area Line Source Algorithm (PAL2.1), the EPA Industrial Source 5 Complex Short Distance 3 (ISCST3) model, and the Argonne National Laboratory Seasonal/Annual Cooling Tower Impact (SACTI) model ((*Carhart and Policastro*, 1991; *Policastro et al.*, 1994) are used. Some of the limitations described above were addressed later in the development of ISC-PRIME and AERMOD-PRIME models in order to replace ISC3 series models ((*Schulman et al.*, 1997; *Petersen*, 2004)). The current trend in modeling for urban air pollution is focused on the improvement of advection in atmospheric dispersion models (atmospheric dispersion models TAPM, Ausplume, and CALPUFF (*Brown and Fletcher*, 2005)) and integrating them with local scale models (see, e.g., the EUROTRAC-2 subproject SATURN; (*Moussiopoulos*, 2010)). These models are currently accepted by regulatory authorities.

In the last decade, new generation of Gaussian dispersion models were introduced with a better description of real physical processes in the atmospheric boundary layer. Examples are the Danish OML model (*Olesen et al.*, 2007), or the British UK-ADMS model (*Carruthers* and *McHugh*, 2009). These often contain integrated systems for different purposes: street canyon models, Gaussian plume models, Eulerian grid models and dispersion model. These model families could give reasonable results in the far field, however, it could give under or overestimation by a factor of two when complex topography and buildings are considered and near filed concentration is a concern (*Mcalpine* and *Ruby*, 2004; *Olesen et al.*, 2007).

CFD based tools have also been used recently to assess plume visibility (*Brown* and *Fletcher*, 2005). Current CFD models however have limited capabilities. They were mostly used to investigate the wind field under steady state conditions, not representing the spatial and temporal variability of the meteorological fields especially around complex terrain (as recognized by *Brown and Fletcher* (2005). They often include assumptions for the vertical atmospheric profiles that do not reflect real conditions (as cautioned by *Presotto et al.* (2005)), and frequently exclude effects of surface vegetation and soil. These issues have been addressed by introducing the transformation method described in (*Kristóf et al.*, 2009; *Rácz et al.*, 2013) and (*Kristóf* and *Balogh*, 2010).

Using the commercial CFD tool ANSYS-FLUENT, continuity, momentum and energy equations are solved based on the finite volume method in an unsteady conservative form. Through user defined functions (UDF), the user can modify the governing equations of the CFD code by adding appropriate source/sink terms to the governing equations (Eqs. $(1)-(6)$). The current adaptation method can also be implemented in other CFD solvers having UDF capabilities such as ANSYS-CFX, StarCD, or the open source solver Openfoam.

$$\nabla \cdot \tilde{v} = 0 , \tag{1}$$

$$\frac{\partial}{\partial t}(\rho_0 \tilde{\mathbf{v}}) + \nabla \cdot (\rho_0\, \tilde{\mathbf{v}} \otimes \tilde{\mathbf{v}}) = -\nabla \tilde{p} + \nabla \cdot \boldsymbol{\tau} + (\tilde{\rho} - \rho_0)\mathbf{g} + \mathbf{F} \tag{2}$$

$$\frac{\partial}{\partial t}(\rho_0 c_p \tilde{T}) + \nabla \cdot (\tilde{v}\, \rho_0\, c_p \tilde{T}) = \nabla \cdot (K_t \nabla \tilde{T}) + S_T , \tag{3}$$

$$\frac{\partial}{\partial t}(\rho_0\, k) + \nabla \cdot (\rho_0\, \tilde{v}\, k) = \nabla \cdot \left(\frac{\mu_t}{\sigma_k} \nabla k\right) + G_k + G_b - \rho_0\, \varepsilon + S_k , \tag{4}$$

$$\frac{\partial}{\partial t}(\rho_0\, \varepsilon) + \nabla \cdot (\rho_0\, \tilde{v}\, \varepsilon) = \nabla \cdot \left(\frac{\mu_t}{\sigma_\varepsilon} \nabla \varepsilon\right) + \rho_0\, C_1\, S\, \varepsilon - \rho_0\, C_{2\varepsilon} \frac{\varepsilon^2}{k + \sqrt{v\,\varepsilon}} + C_{1\varepsilon}\frac{\varepsilon}{k} C_{3\varepsilon} G_b + S_\varepsilon , \tag{5}$$

$$\tilde{\rho} = \rho_0 - \rho_0\, \beta (\tilde{T} - T_0). \tag{6}$$

In the equation system $\tilde{v}, \tilde{p}, \tilde{\rho}, \tilde{T}$ are the transformed field variables of velocity, pressure, density, and temperature. c_p and β are the specific heat capacity of dry air at constant pressure and the thermal expansion coefficient. From the velocity vector ($\tilde{v} = u\,i + v\,j + \tilde{w}\,k$) only the vertical component was affected by the transformation. τ contains the viscous and turbulent stresses, $g = -g\,k$ is the gravitational force per unit, mass and $g = 9.81[\text{N kg}^{-1}]$. Turbulent transport is modeled by the realizable k–ε turbulence model with full buoyancy effects (Eqs. (4)−(5)) developed by *Shih et al.* (1994), where σ_k and σ_ε are the turbulent Prandtl numbers for k and ε, respectively. The turbulent viscosity μ_t and the turbulent heat conduction coefficient K_t are evaluated on the basis of turbulence kinetic energy (k) and dissipation rate (ε) fields. The constant values of $C_{1\varepsilon}$, $C_{2\varepsilon}$, the expressions of C_1 and $C_{3\varepsilon}$, the turbulence production and buoyancy terms G_k and G_b, and the modulus of mean rate-of-strain tensor (S) can be referred either from CFD literature (*Shih et al.*, 1994) or from software documentation (*ANSYS Inc.*, 2013). r_0 and T_0 are reference (sea level) values of density and temperature. Volume sources, responsible for the handling of mesoscale effects, S_T, S_k, and S_ε in Eqs. (3)−(5), as well as vector $F = S_u\,i + S_v\,j + S_w\,k$ in Eq. (2), are functions of local values of field variables. The components of the Coriolis force are included in **F** through S_u, S_v, and S_w.

The interested reader is referred to (*Kristóf et al.*, 2009) and (*Rácz et al.*, 2013) where a full description and validation cases of the transformation method can be found, therefore, further details regarding the basic equations are not given here.

Several authors treated moisture by means of various warm cloud microphysical models of different complexity. These approaches range from simple single-moment (*Kessler*, 1969) and two-moment (*Ziegler*, 1985; *Cohard* and *Pinty*, 2000; *Morrison et al.*, 2005) bulk parameterizations to more complex bin microphysics schemes (*Feingold et al.*, 1994; *Kogan*, 1991; *Ackerman et al.*, 2004). Typically in bulk microphysics, the liquid water is separated into two categories: non-precipitable cloud water and precipitable rain water (*Kessler*, 1969).

2.1. Transport equations

The extended commercial CFD solver we used is essentially closed source, but it is allowed to setup and use arbitrary number of passive scalar equations during the solution. Therefore, in order to describe the phase change, three additional scalar equations (Eqs. (7)−(9)) were considered for the number concentration of cloud condensation nuclei n_{CCN} (in order to track CCN depletion and entrainment effects, where subscript CCN refers to cloud condensation nuclei) and the number of condensed water droplets N_c together with total water content of air q_t. Rain water is currently neglected, since condensation will determine the growth of drops smaller than about 20 μm and no larger droplets are expected during the initial rise of a thermal or during the cooling tower plume rise.

$$\frac{\partial \rho n_{CCN}}{\partial t} + \frac{\partial}{\partial x_i}\left(\rho u_i n_{CCN} - \Gamma \frac{\partial n_{CCN}}{\partial x_i}\right) = \left(S_{n_{CCN}}\right)_{act} + \left(S_{n_{CCN}}\right)_{evap} + \left(S_{n_{CCN}}\right)_{sed}, \tag{7}$$

$$\frac{\partial \rho q_t}{\partial t} + \frac{\partial}{\partial x_i}\left(\rho u_i q_t - \Gamma \frac{\partial q_t}{\partial x_i}\right) = \left(S_{q_t}\right)_{act} + \left(S_{q_t}\right)_{cond/evap} + \left(S_{q_t}\right)_{sed}, \tag{8}$$

$$\frac{\partial \rho N_c}{\partial t} + \frac{\partial}{\partial x_i}\left(\rho u_i N_c - \Gamma \frac{\partial N_c}{\partial x_i}\right) = \left(S_{N_c}\right)_{act} + \left(S_{N_c}\right)_{cond/evap} + \left(S_{N_c}\right)_{sed}, \tag{9}$$

$$q_t = q_v + q_l, \tag{10}$$

where q_v and q_l are the specific humidity of water vapor and liquid water per unit mass. Γ is the diffusion coefficient of the given scalar.

In order to simulate mean sizes and concentrations of droplets in wet plumes, the scheme needs to represent processes that would affect the droplet spectra of the plume (right side of Eqs. (7)−(9)). These are the activation of droplets on condensation nuclei, condensation/evaporation of droplets, entrainment of ambient air (*Warner*, 1969; *Paluch* and *Knight*, 1984; *Brenguier* and *Grabowski*, 1993; *Su et al.*, 1998; *Lasher-trapp et al.*, 2005), and additional activation of droplets (*Warner*, 1969; *Pinsky* and *Khain*, 2002).

The relationship between droplet number (N_c) and liquid water content (q_l) is determined by using a log-normal droplet size distribution function (Eqs. (11)−(12)):

$$n_c(r) = \frac{N_c}{r\sigma_c\sqrt{2\pi}}\exp\left(-\frac{1}{2\sigma_c^2}\left(\ln\frac{r}{r_0}\right)^2\right), \tag{11}$$

$$\bar{r}_3 = r_0 \exp\left(\frac{3}{2}\sigma_c^2\right) \text{ and } \rho q_l = \frac{4}{3}\pi\bar{r}_3^3 \rho_w N_c, \tag{12}$$

where r is the droplet radius, r_0 is the distribution median value, σ_c is the logarithmic standard deviation, $\bar{r}_3$ is the mean mass radius, and ρ_w is the density of water.

Atmospheric aerosols and cloud condensation nuclei play an important role in the condensation of droplets and evolution of clouds. In this study, the method described by *Cohard et al.* (1998) was chosen to describe the relationship between supersaturation and the nucleated number of droplets (N_{CCN}), as it is computationally more efficient, gives more robust estimates (*Grabowski*, 2006), and requires less programming efforts.

$$N_{CCN} = Cs^k F\left(\mu, \frac{k}{2}; \frac{k}{2}+1; -\beta s^2\right), \tag{13}$$

where $C = 3270$ cm^{-3} is a parameter of the nucleation process, s is the supersaturation, F is the hyper-geometric function and $\mu = 0.7$, $\beta = 136$, and $k = 1.56$ are parameters characterizing the aerosol distribution of a continental type of air mass. Eq. (13) is the extension of the simple and famous power law formula of *Twomey* (1959) but improved to give better results from weak to strong supersaturations.

Given the number of nucleated drops, the source term due to nucleation can be calculated assuming heterogeneous nucleation (*Pruppacher et al.*, 1998).

$$\left(S_{N_c}\right)_{act} = \frac{1}{\Delta t}\max\left(N_{CCN,\max} - N_c, 0\right), \tag{14}$$

where Δt is the numerical time step. It is assumed that condensation and evaporation proceed through changes of q_c without any effects on N_c (*Richard and Chaumerliac*, 1989) except during activation of CCN and total evaporation of smaller droplets.

2.2. Droplet growth by activation and diffusion

Once droplets are activated, the two primary components of their growth are the vapor diffusion and collision-coalescence. Since rain water is neglected, only growth by diffusion is considered. The critical radius of newly formed droplets can be calculated according to the Köhler theory (see, e.g., (*Pruppacher et al.*, 1998)).

$$\left(r_{crit}\right)_{act} = \frac{4}{3}M_w\sigma_w R\rho_w T(s/100), \tag{15}$$

where M_w and σ_w are the molecule mass and surface tension of the water substance, R and T are the universal gas constant and the physical temperature of ambient air.

The corresponding source term due to activation for the liquid water content is:

$$\left(S_{q_t}\right)_{act} = \frac{4\pi\rho_w}{3\rho} r_{crit}^3 \left(\frac{\partial N_c}{\partial t}\right)_{act}, \tag{16}$$

The condensation rate can be calculated based on (*Pruppacher et al.*, 1998):

$$\left(S_{q_t}\right)_{cond/evap} = \frac{4\pi r(s - A + B)f_v}{G(T, p)}, \tag{17}$$

where A, B, and f_v express curvature, solute, and ventilation effects and $G(T, p)$ is a term dependent on local thermodynamic variables.

$$A = \frac{2\sigma_w}{R_v T \rho_w r}, \quad B = \frac{\varepsilon v \Phi_s M_w m_a}{M_s (m - \rho_w m_a / \rho_s)}, \quad G(T, p) = \frac{L_v}{k_a T}\left(\frac{L_v}{R_v T} - 1\right) + \frac{R_v T}{p_{sat} D_v}, \tag{18}$$

where ε is the water-soluble fraction of the aerosol, the product $v\Phi_s$ is the van't Hoff factor, ρ_s and m_a are the aerosol density and mass, m is the droplet mass, M_w and M_s are the molecular mass of water and solute, L_v is the latent heat of evaporation, R_v is the specific gas constant of water vapor, k_a and D_v are the modified thermal conductivity and diffusivity of air and water vapor, p_{sat} is the saturated vapor pressure over flat water surface at environmental temperature.

2.3. Partial and total evaporation of droplets

Droplets evaporate once convected to unsaturated regions ($s < 0$). This process is described based on the work of *Chaumerliac et al.* (1987). Due to partial evaporation, drops with a size smaller than a certain threshold (r_{crit}) will be removed from the system, therefore resulting a decrease in N_c. The corresponding source term is:

$$\left(S_{N_c}\right)_{evap} = \frac{1}{\Delta t} \int_0^{r_{crit}} \frac{N_c}{r\sigma_c \sqrt{2\pi}} \exp\left(-\frac{1}{2\sigma_c^2}\left(\ln\frac{r}{r_0}\right)^2\right) dr, \tag{19}$$

where r_{crit} can be calculated as follows:

$$r_{crit} = \sqrt{(-2\ A3^{-1}\ s\ \Delta t)}, \tag{20}$$

$$A3 = \frac{\rho_w R_v T}{p_{sat} D_v} + \frac{L_v \rho_w}{k_a T}\left(\frac{L_v}{R_v T} - 1\right).$$ (21)

Total evaporation of droplets will occur when the calculated mass of evaporated drops is larger than the mass present in the given volume. In this case $Nc = 0$ and the local CCN number is regenerated. The sedimentation terms on the right side of Eqs. (7)–(9) can be used to describe the settling of droplets, however, the settling terms are not considered here, as they are expected to be small in certain plume dispersion cases (*Bouzereau et al.*, 2008).

The superstauration s is calculated based on the saturation pressure (Eq. (22)). It is calculated for flat water surfaces based on the formula of *Bolton* (1980). The expression is accurate to 0.3% for –35 °C < T < 35 °C temperature range.

$$p_{sat} = 6.112 \exp\left(\frac{17.67\,T}{243.5 + T}\right),$$ (22)

where T and p_{sat} are in °C and hPa.

The following expressions give the connection between water vapor mass fraction and vapor pressure:

$$p_v = \left(\frac{q_v}{0.622 + q_v}\right) p,$$ (23)

where p_v and p are the vapor partial pressure and the pressure of moist air.

Finally, the supersaturation is given by the following formula:

$$s = \frac{p_v}{p_{sat}} - 1,$$ (24)

In the following chapter, the transformation and the microphysics scheme will be validated against the simulation of an idealized two-dimensional rising thermal and three-dimensional full scale plume dispersion cases.

3. Results

3.1. Numerical experiments with two-dimensional rising thermals

It is common in the development of microphysical schemes, that researchers test their models' behavior with idealized two-dimensional simulations. A frequently used generic test case is a rising thermal simulation in a stably stratified environment. Two types are common in the literature, one where the development of the thermal is initiated by surface heating (see, e.g., (*Klaassen* and *Clark*, 1985)) and another type when an initial perturbation (potential temperature, vapor content, etc.) is placed in the domain at a certain height. The latter one, described by *Grabowski* and *Clark* (1991), will be used here as a test case for validation, as it allows shorter computation due to not simulating the initial development phase of the thermal.

3.1.1. Rising thermal in a dry stable atmosphere

In order to separate the moist dynamics from discretization effects, the rise of a dry thermal in a Bousinesq fluid was simulated first.

The model domain was 3.6 km wide in the horizontal and 2.4 km in the vertical direction with equidistant mesh resolution. Different grid sizes of 20, 10, 5, 2.5, and 1.25 m were tested in order to see mesh sensitivity of the solution. The lateral boundaries were defined as periodic boundary, the top and bottom boundaries as free slip adiabatic walls. The initial circular perturbation was placed at $x = 0$ km and $z = 0.8$ km with a radius of 500 m and 0.5 K higher initial temperature than the constant ambient temperature 287 K. Third order MUSCL schemes (monotone upstream-centered schemes for conservation laws, (*van Leer*, 1979)) were used when solving the momentum and energy equations, as they can effectively suppress the non-physical oscillations with the introduction of adaptive numerical dissipation into numerical solutions. All transformation source terms in Eqs. (2)−(5) were turned off in this case. The total flow time was 8 min with a time step of 1 s. Results were compared to standard nonoscillatory MPDATA simulations showed in Section 4 in *Margolin et al.* (1997).

At 20 m and lower resolutions, results were starting to degrade rapidly, the interfacial eddies were smeared out (not shown here). A converged solution could be obtained at higher resolutions, the 5, 2.5, and 1.25 m cases were virtually identical (see *Fig. 1*). During the solution, the viscosity was explicitly defined and was varied among the different cases. *Fig. 2* shows that the results are less sensitive to the changes of the predefined viscosity in the investigated range.

Overall, a good correspondence can be found regarding the gross features; the rise height and size of the final shape of the bubble agrees well. There are differences in the fine details, though, the size and position of interfacial eddies slightly differ from the MPDATA solutions.
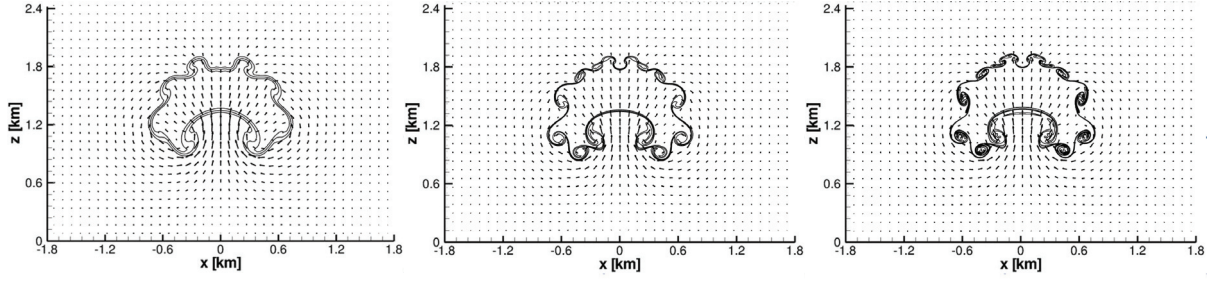
Fig. 1. Mesh sensitivity of the developed interfacial eddies. The equidistant mesh resolution is 20 m, 5 m, 1.25 m from left to right, and the viscosity is 0.5 m^2 s^{-1} for all cases.
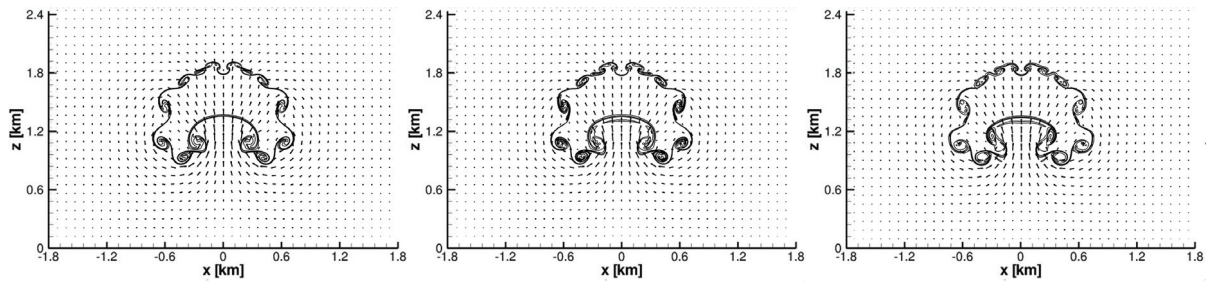

Fig. 2. Sensitivity of the developed interfacial eddies to the viscosity. The viscosity is 1, 0.5, 0.1 m^2 s^{-1} from left to right, and the mesh resolution is 2.5 m for all cases.

3.1.2. Rising of a moist thermal

Model behavior changed significantly when moist dynamics were activated. The domain in this case was the same as above with an equidistant resolution in both spatial directions of 40, 20, 10, 5, 2.5 m. The initial perturbation of relative humidity (*RH* = 100 %) was placed at 0.8 km height with a diameter of 200 m that was smoothly relaxed to the environmental value within approximately 250 m radius. The environmental base state stability and the relative humidity were set to *dlnθ/dz* = 1.3 10^{-5} m^{-1} and 20%, and the perturbation relaxation of *RH* was defined as:

$$RH = 20\% + 80\% \cos^2\left(\frac{\pi}{2}\frac{r - 200}{100}\right), 200\text{m} < r < 300\text{m}. \tag{25}$$

The lateral, top, and bottom boundaries were defined as periodic and free slip adiabatic walls with a temperature of 289 K at the lower surface. The eddy viscosity of the air was explicitly defined and varied between 0.25 and 2 m^2 s^{-1} among the simulation cases.

Third order MUSCL schemes, pressure staggering option (PRESTO) (*ANSYS Inc.*, 2013) were used when solving the momentum and energy equations,

and for pressure interpolation. Results were compared to series of non-oscillatory MPDATA solutions presented in Section 3 in (*Grabowski* and *Clark*, 1991)

The general formation of the liquid water field of the thermal is illustrated in *Fig. 3*. During the initial 4 min of rise, a very good match can be found. This period was weakly affected by the mesh resolution or the predefined viscosity (not shown here). At higher resolutions (5 m and 2.5 m), the model predictions were fairly close to the semi-Lagrangian and Eulerian MPDATA solutions, the overall shape and rise height were similar, the interfacial eddies were well resolved. Differences can be found in the fine details, though, the exact position and shape of interfacial eddies are somewhat different but still close to the semi-Lagrangian model results that is superior in capturing the interface instability (see Section 4a of *Grabowski* and *Smolarkiewicz* (1996)). At low spatial resolutions, the CFD model still captured the overall shape, but the quality degraded quickly, no interfacial eddies could be found at 20 m resolution. However, the erosion of cloud water field was not as strong as the Eulerian MPDATA model showed at the same resolution.

Overall, the model output is in *Figs. 4* and *5* suggest that the results are converging to a common solution, and it is in a good agreement with the MPDATA results. Differences are possibly due to the different numerical schemes and the lack of precipitation scheme in the CFD model.
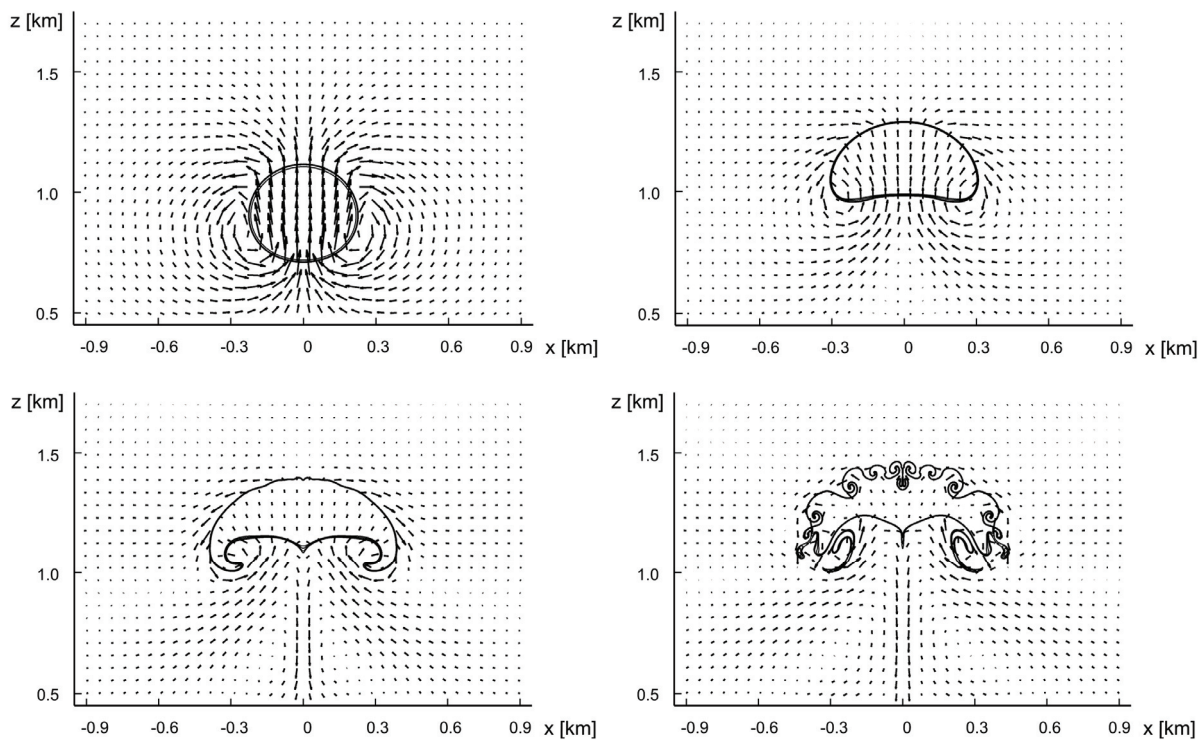

Fig. 3. Development of the initial water vapor perturbation. Isolines of q_l field at $t = 2, 4, 6,$ and 8 min of the moist thermal rise. The viscosity and the mesh resolution are 0.5 m^2 s^{-1} and 2.5 m in each panel. Contour intervals for q_l are 0.05, 0.1, 0.2, and 0.3 g kg^{-1}.
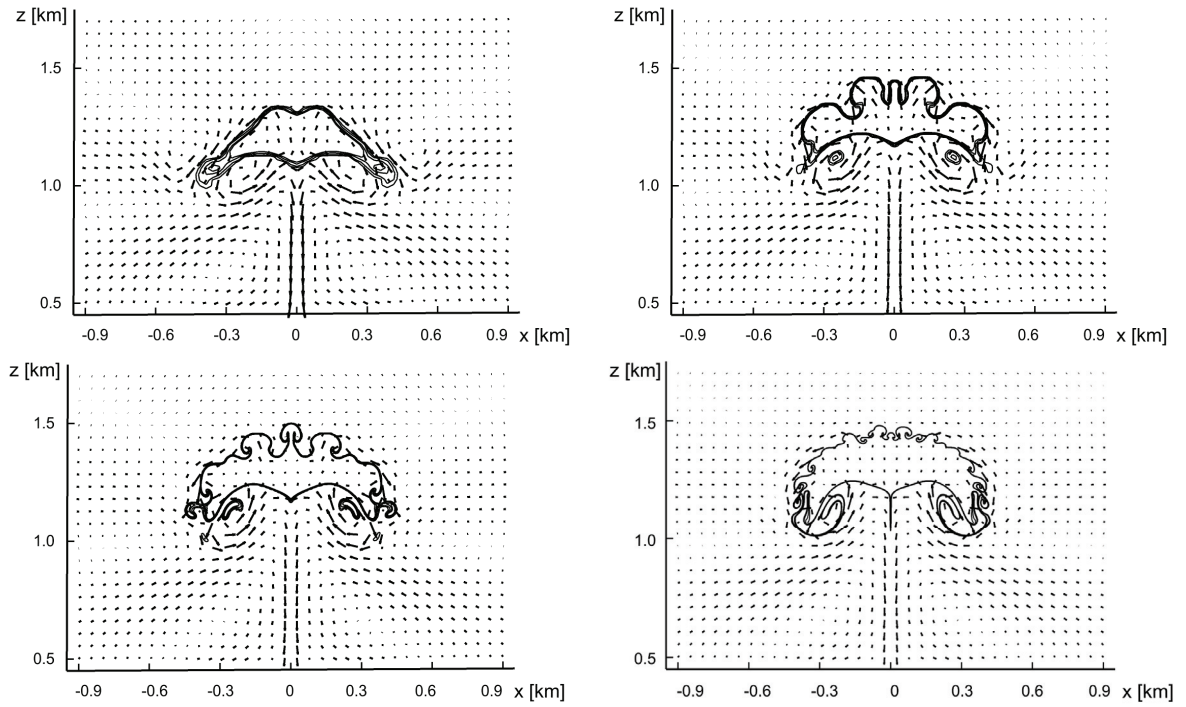
Fig. 4. Same as *Fig. 3.* but for different mesh resolutions. From left to right, the mesh sizes are 20, 10, 5, and 1.25 m. The viscosity is 0.5 m^2s^{-1}.
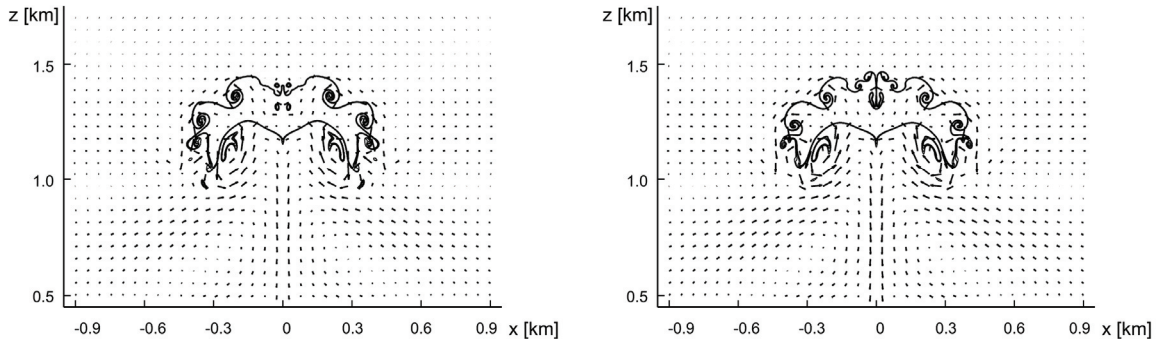

Fig. 5. Same as *Fig. 3* but for different viscosities. Mesh resolution is 2.5 m, viscosity is 0.1 and 0.25 $m^2 s^{-1}$ (from left to right).

3.2. *Simulation of plume formation of a wet cooling tower, the Bugey 1980 field campaign*

In this chapter, the CFD simulation results will be compared to full scale measurement data that was collected during a large measurement survey around wet cooling towers of a nuclear power plant around Bugey, France. Radio-

soundings, droplet spectra, airborne measurements, measurements describing the ambient thermodynamic states as well as photographic records are available for comparision (*Bouzereau et al.*, 2008).

3.2.1. Initial and boundary conditions

During the campaign, very different plume shapes were observed from which two of the characteristic cases were selected for comparison. The first one (March 11, 1980) was characterized by high wind shear, conditionally unstable stratification, and an upper layer with high relative humidity. The second one (March 12, 1980) had lower ambient wind speed, more stable stratification and as a result, smaller horizontal plume extent characterized by sharp plume bent-over.

The domain in both cases covers a 10 km × 4 km area with a total height of 4 km. An equidistant grid was used during the simulations with a resolution of 40 m that was adaptively refined in two steps around the tower and the plume, resulting a minimum grid size of 10 m in critical areas. The interpolated initial and boundary profiles for the domain as well as the plume exit conditions, the vertical velocity, temperature, turbulence profiles, and the liquid water content were based on the radiosoundings and previous calculations of *Bouzereau et al.* (2008) (see *Fig. 6* for the atmospheric profiles and *Table 1* for tower exit conditions). Turbulent kinetic energy k and its dissipation ε at the tower exit were set to 1.7 $m^2 s^{-2}$ and 0.07 $m^2 s^{-3}$ in both cases. Droplet number concentration at the tower exit was deduced from measurements, i.e., $N_c = 10^4$ cm^{-3}. The nucleation parameterization was after *Cohard et al.* (1998) using parameters for a continental type of air mass, i.e., $C = 3270$ cm^{-3}, $k = 1.56$, $\mu = 0.70$, $\beta = 136$, and $\sigma_c = 0.28$. The time step was 1 s and the total integration time was 3600 s in both cases.

Table 1. Plume exit conditions for March 11 and 12, 1980. Exit conditions for the towers 4E–W and 5E–W are given separately. Subscript "env" refers to environmental values. The tower exit temperature ΔT is given compared to the environmental values. w and q_l are the vertical velocity component and the liquid water content, respectively, at the tower exit.

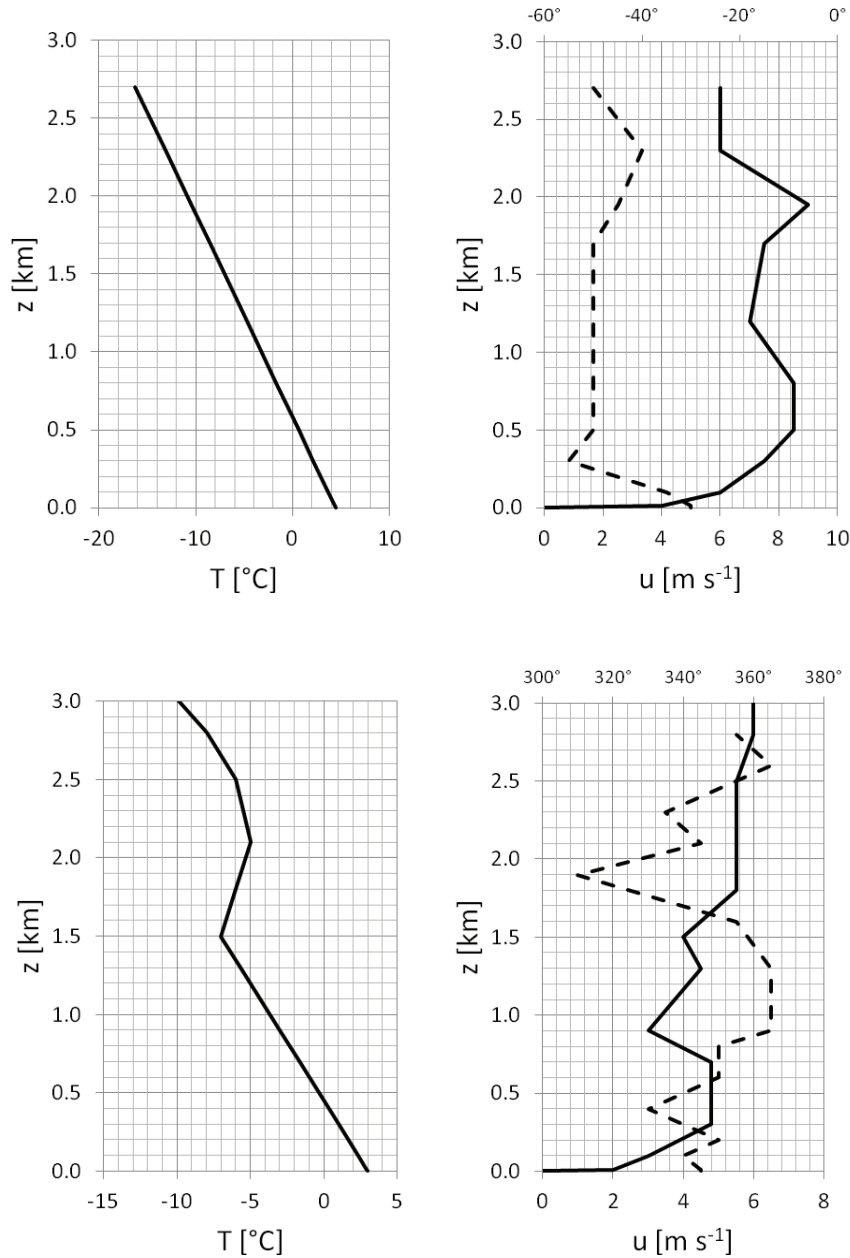| Tower exit conditions	q_l [g kg^{-1}]		ΔT [°C]		w [ms^{-1}]		T_{env} [°C]	p_{env} [Pa]
	4E-W	5E-W	4E-W	5E-W	4E-W	5E-W		
March 11	0.889	0.719	18.34	17.77	3.8	3.73	4.44	97771
March 12	0.8	0.8	18.2	17.7	3.8	3.7	3.31	97994

Fig. 6. Ambient initial and boundary conditions for the March 11, 1980 (top) and March 12, 1980 (bottom) cases. Left panel: ambient temperature. Rigth panel: wind speed (solid line) and wind direction (dashed line).

3.2.2. Simulation results of plume formation

Moist air is injected at the tower exit into the atmosphere characterized by strong shear with a high relative humidity upper layer, resulting in a periodic cumulus like plume formation farther downstream of the tower. This phenomena is well captured by the CFD code compared to visual observations and existing calculations (see Chapter 4 and Appendix A of *Bouzereau et al.* (2008)). The

oscillation in the liquid water content (LWC) field observed as rising thermals in *Fig. 7.* shows a wave length of about the same as the model output of the MERCUR code presented in *Bouzereau et al.* (2008) and of the observations. The first thermal-like structure appears closer downstream of the tower in the CFD model, that could be explained by differences in the turbulence level, and by the effect of higher resolution mesh in critical areas.
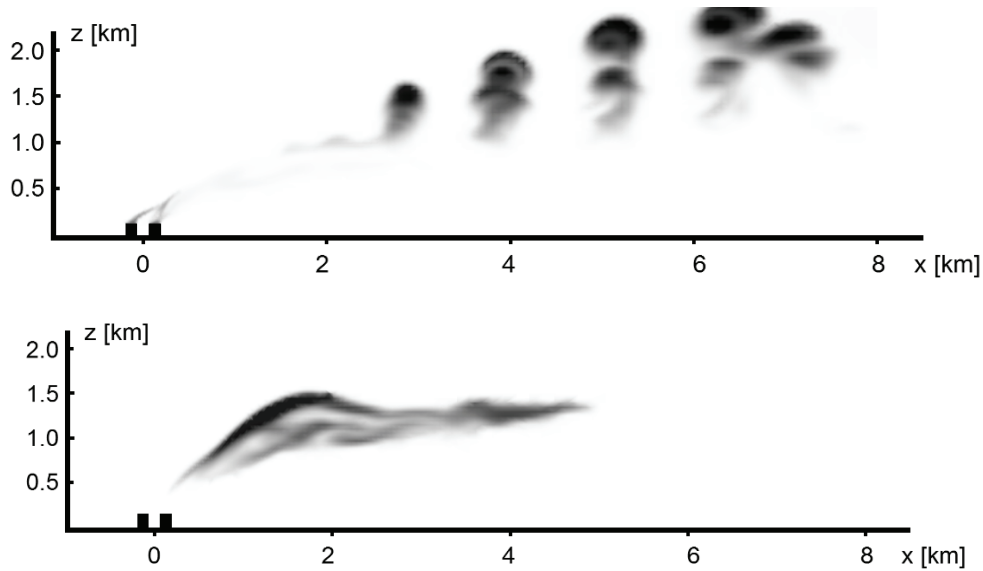

Fig. 7. Volume rendering of the LWC field of the simulated plumes, March 11, 1980 (top) and March 12, 1980 (bottom). The field is transparent below $q_l = 0.01$ g kg^{-1} and opaque when higher than 1.0 g kg^{-1} with 0.1 g kg^{-1} steps in the opacity.

A quantitative comparison is shown in *Fig. 8* where CFD model output is plotted against available aircraft data. In order to obtain valuable results on plume formation and dispersion, it is important to have good initial data on the vertical thermal structure as well as wind shear and humidity. The temperature field was well captured by the simulation, it follows the ambient temperature profile, and the aircraft data lies well between the simulated extremum. The maximum simulated values of LWC field were also compared to recorded data during the campaign. Although aircraft data for LWC was not available for comparison for the initial rise, in the layer between 900 m and 1800 m the simulation compares well, tendencies in liquid water field are well captured for the high wind case with a slight overestimation along the plume axis. During aircraft data sampling, data for instantaneous vertical velocity was also collected. This cannot be compared directly to simulation output, as vertical velocity from URANS simulations does not contain the fluctuation component of the wind speed. However, it is possible to deduce approximate values from the turbulence kinetic energy field. The survey shows significant fluctuations in the velocity field, which is also well reflected in the simulation results.

248

The simulated plume height could be extracted from *Fig. 8*, where the liquid water content is starting to drop significantly. The simulation showed slight overestimation for the high wind case, it gave values between 2000 m and 2500 m, while during the survey a height of ~1950 m and ~2250 m was observed.

In general, the model showed good overall performance with the CFD model improved with the bulk microphysical scheme. Further steps will include the implementation of sedimentation and precipitation schemes.
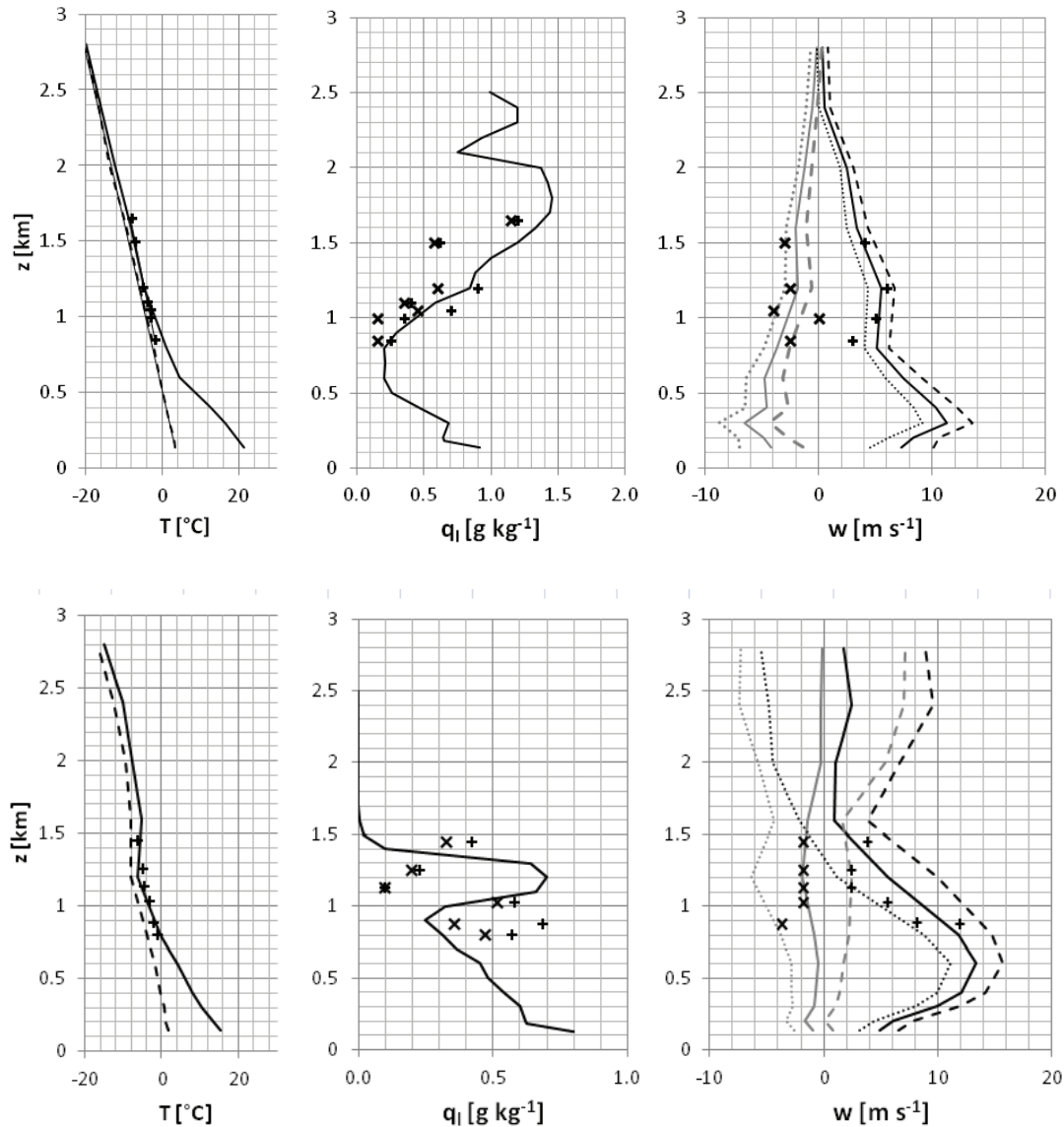

Fig. 8. Simulation results for March 11, (top panels) and March 12,1980 (bottom panels) compared to the aircraft measurements. On the left: maximum (solid line) and minimum (dashed line) of the simulated temperature. Symbols: measured temperature average through the plume. Center: predicted maximum of the LWC field (solid line) at each level. Symbols: 'x' and '+' represent the measured minimum and maximum of the LWC. Right panels: simulated vertical velocity *w* (solid lines: maximum in black, minimum in grey). Doted and dashed lines show the fluctuation components. Symbols: 'x' and '+' represent the minimum and maximum instantaneous vertical velocities observed at each flight level.

4. Summary and conclusions

A transformation method was developed in the past in order to extend the capabilities of commercial CFD solvers with mesoscale effects. Thermal stratification, adiabatic cooling caused by hydrostatic pressure driven expansion, compressibility, and Coriolis force were taken into account with the help of a transformation system and customized volume sources applied to the governing equations. In this paper further advances were shown. A bulk warm microphysical scheme was implemented in the solver in order to simulate humidity transport and phase change in atmospheric flows.

Model results were successfully validated with the rise of idealized two-dimensional dry and wet thermals. We have then applied the model to the simulation of wet plume formation originated from a cooling tower of a large nuclear power plant.

Results obtained from our simulations are encouraging with regard to the predictability of cumulus-like plume structures in the far field of the tower formed in complex wind field and thermal stratification, the overall liquid water content along the plume axis, and also the turbulent fluctuations caused by the vertical movements in the plume.

Using only one single unstructured grid and a uniform physical description for close- and far-field flow, one can take the advantage of the model adaption in the simulation of mesoscale atmospheric phenomena. In a single framework, one can investigate the finely structured microscale flow around complex geometrical features, such as flow around buildings with pollution dispersion or study the close- and far-field of wet cooling tower plumes and its effects to the environment.

References

Ackerman, A. S., Kirkpatrick, M. P., Stevens, D. E., and *Toon, O. B.*, 2004: The impact of humidity above stratiform clouds on indirect aerosol climate forcing. *Nature 432*, 1014–1017.

Al-Waked, R., and Behnia, M., 2006: CFD simulation of wet cooling towers. *Appl. Therm. Eng. 26*, 382–395.

ANSYS Inc., 2013: FLUENT 13 documentation. In: Fluent User Services Center.

Balczó, M., Balogh, M., Goricsán, I., Nagel, T., Suda, J., and *Lajos, T.*, 2011: Air quality around motorway tunnels in complex terrain–Computational Fluid Dynamics modeling and comparison to wind tunnel data. *Időjárás 115*, 179–204.

Barber, F., Martin, A., Shepherd, J., and *Spurr, G.*, 1974: The persistence of plumes from natural draft cooling towers. *Atmos. Environ. 8*, 407–418.

Bolton, D., 1980: The computation of equivalent potential temperature. *Mon. Weather Rev. 108*, 1046–1053.

Bouzereau, E., Musson Genon, L., and *Carissimo, B.*, 2008: Application of a semi-spectral cloud water parameterization to cooling tower plumes simulations. *Atmos. Res. 90*, 78–90.

Brenguier, J.-L., and *Grabowski, W. W.*, 1993: Cumulus entrainment and cloud droplet spectra: A numerical model within a two-dimensional dynamical framework. *J. Atmos. Sci. 50*, 120–136.

Briggs, G. A., 1975: Plume rise predictions. *Lect. Air Pollut. Environ. Impact Anal. AS, 59-l 1.*

Briggs, G. A., 1984: Plume rise and buoyancy effects. *Atmos. Sci. Power Prod.* 327–366.

Brown, G. J., and Fletcher, D. F., 2005: CFD prediction of odour dispersion and plume visibility for alumina refinery calciner stacks. *Process Saf. Environ. Prot. 83*, 231–241.

Campistron, B., 1987: Interaction between a natural snowfall and a cooling tower plume: An experimental study with a millimetric Doppler radar. *Atmos. Environ. 21*, 1375–1383.

Carhart, R. A. and *Policastro, A. J.*, 1991: A second-generation model for cooling tower plume rise and dispersion—I. Single sources. *Atmos. Environ. Part A. Gen. Top. 25*, 1559–1576.

Carruthers, D. and *McHugh, C.*, 2009: Comparison of ADMS and AERMOD meteorological preprocessor and dispersion algorithms. Proc. Air Waste Manag. Assoc. Air Qual. Model. Next Gener. Model.

Chaumerliac, N., Richard, E., Pinty, J.-P., and *Nickerson, E. C.*, 1987: Sulfur scavenging in a mesoscale model with quasi-spectral microphysics: Two-dimensional results for continental and maritime clouds. *J. Geophys. Res. Atmos. 92*, 3114–3126.

Cohard, J., Pinty, J., and *Bedos, C.*, 1998: Extending Twomey's analytical estimate of nucleated cloud droplet concentrations from CCN spectra. *J. Atmos. Sci., 55,* 3348–3357.

Cohard, J.-M. and *Pinty, J.-P.*, 2000: A comprehensive two-moment warm microphysical bulk scheme. I: Description and tests. *Q. J. Roy. Meteorol. Soc. 126*, 1815–1842.

Csanady, G. T., 1973: Turbulent diffusion in the environment. D. Reidel Pub. Co.,.

Davidson, G. A., 1989: Simultaneous trajectory and dilution predictions from a simple integral plume model. *Atmos. Environ. 23*, 341–349.

Davidson, G. A., 1994: Dimensionless correlations for buoyant plume behaviour in cross-flows and scaling criteria for physical modeling of dispersion processes. *J. Wind Eng. Ind. Aerodyn. 51*, 135–155.

Feingold, G., Stevens, B., Cotton, W. R., and *Walko, R. L.*, 1994: An explicit cloud microphysics/LES model designed to simulate the Twomey effect. *Atmos. Res. 33*, 207–233.

Gangoiti, G., Sancho, J., Ibarra, G., Alonso, L., García, J. A., Navazo, M., Durana, N., and *Ilardia, J. L.*, 1997: Rise of moist plumes from tall stacks in turbulent and stratified atmospheres. *Atmos. Environ. 31*, 253–269.

Grabowski, W. W., 2006: Indirect impact of atmospheric aerosols in idealized simulations of convective – radiative quasie quilibrium. *J. Clim. 19*, 4664–4682.

Grabowski, W. W., and *Clark, T. L.*, 1991: Cloud–environment interface instability: Rising thermal calculations in two spatial dimensions. *J. Atmos. Sci. 48*, 527–546.

Grabowski, W. W., and *Smolarkiewicz, P. K.*, 1996: Two-time-level semi-Lagrangian modeling of precipitating clouds. *Mon. Weather Rev. 124*, 487–497.

Greig, J. E., Carnie, J. A., Tallis, G. F., Ryan, N. J., Tan, A. G., Gordon, I., Zwolak, B., Leydon, J. A., Guest, C. S., and *Hart, W. G.*, 2004: An outbreak of Legionnaires' disease at the Melbourne Aquarium, April 2000: Investigation and case-control studies. *Med. J. Aust. 180*, 566–572.

Hanna, S. R., 1972: Rise and condensation of large cooling tower plumes. *J. Appl. Meteorol. 11*, 793–799.

Hanna, S. R., 1976: Predicted and observed cooling tower plume rise and visible plume length at the John E. Amos power plant. *Atmos. Environ. 1967 10*, 1043–1052.

Hanna, S. R., Briggs, G. A., and Hosker, R. P. J., 1982: *Handbook on Atmospheric Diffusion.*

Huff, F. A., 1972: Potential augmentation of precipitation from coolingtower effluents. *Bull. Am. Meteorol. Soc. 53*, 639–644.

Janicke, U., and Janicke, L., 2001: A three-dimensional plume rise model for dry and wet plumes. *Atmos. Environ. 35*, 877–890.

Kessler, E., 1969: On the distribution and continuity of water substance in atmospheric circulations. *Meteor. Monogr., Amer. Meteor. Soc. No. 32*, 84.

Klaassen, G. P. and *Clark, T. L.*, 1985: Dynamics of the cloud-environment interface and entrainment in small cumuli: Two-dimensional simulations in the absence of ambient shear. *J. Atmos. Sci. 42*, 2621–2642.

Kloppers, J. C. and *Kröger, D. G.*, 2005: Influence of temperature inversions on wet-cooling tower performance. *Appl. Therm. Eng. 25*, 1325–1336.

Kogan, Y. L., 1991: The simulation of a convective cloud in a 3-D model with explicit microphysics. part I: Model description and sensitivity experiments. *J. Atmos. Sci. 48*, 1160–1189.

Kristóf, G. and *Balogh, M.*, 2010: Fine scale simulation of turbulent flows in urban canopy layers. *Időjárás 114*, 135–148.

Kristóf, G., Rácz, N., and *Balogh, M.*, 2009: Adaptation of pressure based CFD solvers for mesoscale atmospheric problems. *Bound.-Lay. Meteorol. 131*, 85–103.

Lasher-trapp, S. G., Cooper, W. A., and *Blyth, A. M.*, 2005: Broadening of droplet size distributions from entrainment and mixing in a cumulus cloud. *Q. J. Roy. Meteorol. Soc. 131*, 195–220.

Van Leer, B., 1979: Towards the ultimate conservative difference scheme. V. A second-order sequel to Godunov's method. *J. Comput. Phys. 32*, 101–136.

Lewis, W. K., 1922: The evaporation of liquid into gas. *Trans ASME 44*, 325–340.

Lohasz, M. M., and *Csaba, G.*, 2012: Investigation of exit loss of cooling towers at different wind speeds and Archimedes numbers. Proceeding of THMT-12. Proceedings of the Seventh International Symposium On Turbulence, Heat and Mass Transfer Palermo, Italy, 24-27 September, 2012, Connecticut, Begellhouse, 11.

Lucas, M., Martínez, P. J., Ruiz, J., Kaiser, A. S., and *Viedma, A.*, 2010: On the influence of psychrometric ambient conditions on cooling tower drift deposition. *Int. J. Heat Mass Transf. 53*, 594–604.

Margolin, L., Reisner, J. M., and *Smolarkiewicz, P. K.*, 1997: Application of the volume-of-fluid method to the advection–condensation problem. *Mon. Weather Rev. 125*, 2265–2273.

Mcalpine, J. D. and *Ruby, M.*, 2004: Using CFD to study air quality in urban microenvironments. Environmental Sciences and Environmental Computing. Vol. II, P. Zannetti, Ed., Vol. II of, The EnviroComp Institute, 1–31.

Meroney, R., 2006: CFD prediction of cooling tower drift. *J. Wind Eng. Ind. Aerodyn. 94*, 463–490.

Mochida, A., Murakami, S., Ojima, T., Kim, S. J., Ooka, R., and *Sugiyama, H.*, 1997: CFD analysis of mesoscale climate in the Greater Tokyo area. *J. Wind Eng. Ind. Aerodyn. 67-8*, 459–477.

Mokhtarzadeh-Dehghan, M. R., König, C. S., and *Robins, a. G.*, 2006: Numerical study of single and two interacting turbulent plumes in atmospheric cross flow. *Atmos. Environ. 40*, 3909–3923.

Morrison, H., Curry, J. A., and *Khvorostyanov, V. I.*, 2005: A new double-moment microphysics parameterization for application in cloud and climate models. Part I: description. *J. Atmos. Sci. 62*, 1665–1677.

Moussiopoulos, N., 2010: Air quality in cities: SATURN: EUROTRAC-2 Subproject final report. Springer, Berlin,.

Netterville, D. D. J., 1990: Plume rise, entrainment and dispersion in turbulent winds. *Atmos. Environ. Part A. Gen. Top. 24*, 1061–1081.

Olesen, H. R., Berkowicz, R., Ketzel, M., and *Løfstrøm, P.*, 2007: Validation of OML, AERMOD/PRIME and MISKAM using the Thompson wind tunnel data set for simple stack-building configurations. 6th International Conference on Urban Air Quality, Cyprus, March 27-29, 2007.

Ooka, R., Sato, T., Harayama, K., Murakami, S., and *Kawamoto, Y.*, 2010: Thermal energy balance analysis of the Tokyo metropolitan areausing a mesoscale meteorological model incorporating anurban canopy model. *Bound.-Lay. Meteorol. 138*, 77–97.

Otte, T. L., Lacser, A., Dupont, S., and *Ching, J. K. S.*, 2004: Implementation of an urban canopy parameterization in a mesoscale meteorological model. *J. Appl. Meteorol. 43*, 1648–1665.

Overcamp, T. J, and *Hoult, D. P.*, 1971: Precipitation in the wake of cooling towers. *Atmos. Environ. 5*, 751–765.

Paluch, I. R., and *Knight, C. A.*, 1984: Mixing and the evolution of cloud droplet size spectra in a vigorous continental cumulus. *J. Atmos. Sci. 41*, 1801–1815.

Petersen, R. L., 2004: ISC3 and PRIME versus wind tunnel observations for a power plant with hyperbolic cooling towers. 13th Conference on the Applications of Air Pollution Meteorology, Fifth Conference on Urban Environment, Vancouver, BC 23-26 August 2004.

Pinsky, M. B., and Khain, A. P., 2002: Effects of in-cloud nucleation and turbulence on droplet spectrum formation in cumulus clouds. *Q. J. Roy. Meteor. Soc. 128*, 501–533.

Policastro, A. J., Dunn, W. E., Breig, M., and *Ziebarth, J.*, 1978: Comparison of ten drift deposition models to field data acquired in the Chalk Point dry tracer experiment. Environmental Effects of Cooling Tower Plumes, Symposium on (Supplement),May 2-4, 1978, U. ofMaryland, 76–84.

Policastro, A. J., Dunn, W. E., and *Carhart, R. A.*, 1994: A model for seasonal and annual cooling tower impacts. *Atmos. Environ. 28*, 379–395.

Presotto, L., Bellasio, R., and *Bianconi, R.*, 2005: Assessment of the visibility impact of a plume emitted by a desulphuration plant. *Atmos. Environ. 39*, 719–737.

Pruppacher, H. R., Klett, J. D., and *Wang, P. K.*, 1998: Microphysics of Clouds and Precipitation. *Aerosol Sci. Technol. 28*, 381–382.

Rácz, N., Kristóf, G., and *Weidinger, T.*, 2013: Evaluation and validation of a CFD solver adapted to atmospheric flows: Simulation of topography-induced waves. *Időjárás 117*, 239–275.

Richard, E., and *Chaumerliac, N.*, 1989: Effects of different rain parameterizations on the simulation of mesoscale orographic precipitation. *J. Appl. Meteorol. 28*, 1197–1212.

Robinson, C. S., 1923: The design of cooling towers. *Mech Eng 15*, 99–102.

Schatzmann, M., and *Policastro, A. J.*, 1984: An advanced integral model for cooling tower plume dispersion. *Atmos. Environ. 18*, 663–674.

Schulman, L. L., Strimaitis, D. G., and *Scire, J. S.*, 1997: Addendum to ISC3 user's guide: the prime plume rise and building downwash model.

Shih, T. H., Liou, W. W., Shabbir, A., Yang, Z., and *Zhu, J.*, 1994: A new k-epsilon eddy viscosity model for high Reynolds number turbulent flows: Model development and validation. *Comput. Fluids 24*, 227–238.

Slawson, P. R. and *Csanady, G. T.*, 1967: On the mean path of buoyant, bent-over chimney plumes. *J. Fluid Mech. 28*, 311–322.

Spillane, K. T. and *Elsum, C. C.*, 1983: Prediction of cloud effects in chimney plumes. *Atmos. Environ. 17*, 983–990.

Sturman, A. and *Zawar-Reza, P.*, 2011: Predicting the frequency of occurrence of visible water vapour plumes at proposed industrial sites. *Atmos. Environ. 45*, 2103–2109.

Su, C.-W., Krueger, S. K., McMurtry, P. A., and *Austin, P. H.*, 1998: Linear eddy modeling of droplet spectral evolution during entrainment and mixing in cumulus clouds. *Atmos. Res. 47–48*, 41–58.

Twomey, S., 1959: The nuclei of natural cloud formation part II: The supersaturation in natural clouds and the variation of cloud droplet concentration. *Geofis. Pura e Appl. 43*, 243–249.

Tyagi, S. K., Pandey, a. K., Pant, P. C., and *Tyagi, V. V.*, 2012: Formation, potential and abatement of plume from wet cooling towers: A review. *Renew. Sustain. Energy Rev. 16*, 3409–3429.

Wang, J., Wang, S., Xu, X., and *Xiao, F.*, 2009: Evaluation of alternative arrangements of a heat pump system for plume abatement in a large-scale chiller plant in a subtropical region. *Energy Build. 41*, 596–606.

Wang, S. W., Tyagi, S. K., Sharma, A., and *Kaushik, S. C.*, 2007: Application of solar collectors to control the visible plume from wet cooling towers of a commercial building in Hong Kong: A case study. *Appl. Therm. Eng. 27*, 1394–1404.

Warner, J., 1969: The microstructure of cumulus cloud. Part I. general features of the droplet spectrum. *J. Atmos. Sci. 26*, 1049–1059.

Wei, Q. D., Zhang, B. Y., Liu, K. Q., Du, X. D., and *Meng, X. Z.*, 1995: A study of the unfavorable effects of wind on the cooling efficiency of dry cooling towers. *J. Wind Eng. Ind. Aerodyn. 54-55*, 633–643.

Weil, J. C., 1974: The Rise of moist, buoyant plumes. *J. Appl. Meteorol. 13*, 435–443.

Wigley, T. M. L., and *Slawson, P. R.*, 1971: On the condensation of buoyant, moist, bent-over plumes. *J. Appl. Meteorol. 10*, 253–259.

Xu, X., Wang, S., and *Ma, Z.*, 2008: Evaluation of plume potential and plume abatement of evaporative cooling towers in a subtropical region. *Appl. Therm. Eng. 28*, 1471–1484.

Yamada, T., 2003: Numerical simulation of airflows around buildings by using a mesoscale atmospheric model. Air & Waste Management Associations 96th Annual Conference and Exhibition, San Diego, California, June 23 - 25, 2003, San Diego, California.

Ziegler, C. L., 1985: Retrieval of thermal and microphysical variables in observed convective storms. Part 1: Model development and preliminary testing. *J. Atmos. Sci. 42*, 1487–1509.